Improvement of Corrosion Resistance of Rolled and Heat-treated AA6111 Alloys with Zirconium addition

Saba Jameel Hassan
Department of Metallurgical Engineering, Materials Engineering College, Babylon, University, Babil, Iraq.
Email: sabajmeel1228@gmail.com
Basem Al-Zubaidy
Department of Metallurgical Engineering, Materials Engineering College, Babylon, University, Babil, Iraq.
Email: mat.basem.mahsn@uobabylon.edu.iq
SaadHameed Al-Shafaie
Department of Metallurgical Engineering, Materials Engineering College, Babylon, University, Babil, Iraq.
Email:mat.saad.hameed@uobabylon.edu.iq

ABSTRACT

The zirconium addition effect on the corrosion behavior of the AA6111 alloy was investigated. All alloys were produced by the stir-casting method. Homogenization heat treatment (at 500 ºC for 8 hours) was performed on the AA6111 alloy only. The alloys were solutionized (at 540 ºC for 30 minutes) and artificially aged (at 180 ºC for 10 hours). Particle size measurements, XRD, energy-dispersive X-ray spectroscopy (EDS), open circuit potential (OCP)-time measurement, and potentiodynamic polarization were performed for all samples. The microstructure analysis displayed different fine intermetallic phases distributed in large amounts in the AA6111+0.54%Wt%Zr alloy compared to the AA6111 alloy. From the results of electrochemical tests, it is clear that the addition of zirconium to the AA6111 alloy has led to a significant and noticeable improvement in corrosion resistance, as the improvement rate reached 72.53%. Compared to the AA6111 alloy without adding zirconium.

KEYWORDS: AA6111 aluminum alloy; Al-Mg-Si-Zr alloys; corrosion behavior; particle size; Potentiodynamic polarization.

1. INTRODUCTION

Because of the protective properties of the aluminum oxide passive film that spontaneously forms, pure aluminum is typically thought to be corrosion-resistant**[1,2]**. Since it has a large band-gap, the passive film is not a strong supporter of electrochemical reactions. On pure Al, even a small scratch or local breakdown of the passive layer would only cause a modest cathodic current to sustain the local anodic attack from the remaining surface oxide. Through suitable alloying additions and heat treatments, certain microstructures are created in Al alloys to enhance their mechanical properties**[1,3,4]**.Most Al alloys are sensitive to localized corrosion due to intermetallic particles (IMPs) formed during alloying and subsequentheat treatment, which may operate as active sites for film breakdown or efficient cathodes for anodic attack. In most situations, the continuous matrix and IMPs in Al alloys have differing electrochemical properties, which may lead to localized corrosion. Localized corrosion start is often related to IMPs serving as local cathodes, promoting the oxygen reduction process

(ORR) and causing dissolution or pitting attack at the particle-matrix interface or surrounding area**[1,5].**

AA6xxx aluminum alloys are a sort of heat-treatable alloys that consist primarily of magnesium (Mg) and silicon (Si) as the main alloying components. Their primary method of strengthening is by age hardening, which leads to the formation of Mg2Si **[6]** precipitates. AA6xxx alloys are renowned for their exceptional specific strength, formability, and plasticity. As a consequence, they have been widely used in the infrastructure, vehicle, and equipment sectors**[6].** The automobile industry aims to achieve fuel conservation by reducing vehicle weight via the use of lighter materials, such as aluminum alloys**[7]**. AA6xxx often demonstrates excellent corrosion resistance. Nevertheless, in situations when AA6xxx alloys are subjected to harsh conditions such as road deicing salts, marine atmospheres, dirt, and other environmental contaminants, they are prone to localized corrosion**[8].**

Multiple authors have investigated the impact of age treatment and composition on the susceptibilities of AA6xxx alloys to corrosion, primarily in acidic chloride solutions. Larsen et al. observed the phenomenon of segregation of a continuous Nano-film rich in copper along the grain boundaries in the under-aged state. This segregation resulted in the formation of a region depleted of solute near grain boundaries. As a consequence, micro-galvanic coupling occurred, leading to preferential attack**[9,10].** In their study, Duan et al. **[11]**examined the intergranular corrosion (IGC) behavior of extruded 6005A alloy profiles with various microstructures. They discovered that the peripheral coarse grain (PCG) structure exhibited a distinct IGC behavior, with less severe pitting corrosion and subsequent IGC compared to the partial recrystallized grain (PRG) structure. Additionally, the PCG structure avoided the transformation into intragranular corrosion, as observed in the PRG structure.In their study, Xuehong et al. **[12]**examined how interrupted aging treatment affects the mechanical properties and intergranular corrosion (IGC) behavior of Al-Mg-Si alloy. They discovered that the interrupted aging T6I6 alloys exhibit simultaneous improvements in mechanical properties (such as strength and elongation) and IGC resistance, in contrast to the T6 alloys.Xuehong et al. **[13]**examined the implications of quenching treatment on the rate of corrosion and mechanical properties of an aluminum 6061 alloy. They found that the treated alloy's mechanical properties and the resistance to corrosion improved as the period of aging increased, which was attributed to the creation of (CuAl2) and (Mg2Si) phases.Onat, A **[14]**researched the corrosion performance of 6xxx series aluminum alloys, focusing on the influence of slight variations in composition and microstructure. The researcher conducted a study on the corrosion characteristics of three aluminum alloys, namely AA6111, AA6451, and AA6016. The results revealed that AA6111, which mainly consists of α (Al 15 (Fe, Mn) 3 Si 2) intermetallic particles (IMPs), exhibited the most favorable corrosion performance. On the other hand, AA6016, which primarily contains β (Al 8 Fe 2 Si) IMPs, showed the least desirable overall corrosion behavior.

As current science and technology advance, the environment in which aluminum components are employed has gotten harsher, and there is a pressing need for improved performance of these components. The objective of this research is to improve the corrosion resistance of the AA6111 alloy by using Zirconium alloying element, followed by homogenization heat treatment, cold rolling, solution heat treatment, quenching, and artificial aging treatments.

2. EXPERIMENTAL PART

The primary alloy used in this investigation was a sheet of AA6111-T4, whose chemical composition is shown in **Table 1**. This alloy's mean Vickers micro-hardness is 89 HV. The

zirconium and nickel powders were obtained from Changsha Xinkang Advanced Materials Co, Ltd. These powders had a median particle size of 20-30 (μm) and a purity of 99.9%.

Three test alloys were fabricated by the process of stir casting, utilizing a Mini MF induction melting furnace. These alloys are included in **Table 1**. The casting procedure included the melting of the AA6111-T4 alloy in a graphite crucible and its subsequent maintenance at a temperature of 720 °C. The liquefied mixture was agitated at a velocity of 200 revolutions per minute using a stirrer equipped with four stainless steel blades for a duration of 5 minutes while being protected by a layer of argon gas. Aluminum foil was used to cover powders before adding them to the melt, based on their weight %. The molten metal was placed over a highly heated metallic mold. The cast, which had dimensions of 200mm in length, 25mm in width, and 7.5mm in thickness, had a homogenizing heat treatment at 500 °C for 8 hours in an SRJX-5-13 Model Box-Resistance Furnace. Afterward, the surface of the tested plates was milled by 3mm of its thickness. Subsequently, the samples underwent rolling at a consistent speed of 32 revolutions per minute (rpm) at room temperature. The roller used had a diameter of 27cm. The rolling process is iterated for 14 passes, resulting in a decrease of 2.5% in thickness with each pass until a reduction rate of 35% of the original thickness is achieved. Following the completion of the rolling process, the rolled sheets underwent solution heat treatment at a temperature of 540°C for duration of 30 minutes. Subsequently, they were rapidly cooled by immersing them in ice for period of 5 minutes. Subsequently, the therapy was accompanied by artificial aging at a temperature of 180 °C for duration of 10 hours. The AA6111 alloy, as well as its variation with added percentage of Wt%Zr was subjected to chemical composition analysis following the ASTM-E1251-17a standard.

Table 1. displays the nominal chemical composition of the produced alloys.

Alloy	Si%	Mg%	Cu%	Fe%	Zr%
AA6111	0.685	0.722	0.969	0.43	0.007
AA6111+Zr	0.697	0.678	0.982	0.35	0.54

Furthermore, these alloys underwent microstructure observation,Particle size measurements,XRD, energy-dispersive X-ray spectroscopy (EDS), open circuit potential (OCP)-time measurement, and potentiodynamic polarization.

Specimens in different cases were prepared for metallography tests using the conventional metallography preparation method, which involves many grinding and polishing procedures. Following the completion of all processing steps for the prepared alloys, including homogenization treatment (only for AA6111 alloy), cold rolling, solution treatment, quenching, and artificial aging, The microstructure of the surface was captured with the YJEYE01 optical microscope.The particle size was also measured using Image-J and Origin-Pro 2024b analysis programs based on the microstructure images. In addition,The XRD analysis was used to determine the stoichiometry of secondary phases present in the matrix of AA6111 and AA6111+0.54%Wt%Zr aged alloys and their relative proportions. The average chemical composition of the specimen's micrograph after artificial aging was determined using Energy Dispersive Spectroscopy (EDS) based on the number and distribution of its components.

The presence of residual stresses, the high density of dislocations, and the presence of precipitation particles on the grain boundaries may significantly affect the corrosion performance of the alloys. Corrosion tests were conducted using the open circle test to understand the corrosion behavior of these alloys by immersing the samples in a solution of 3.5% sodium chloride for the period (0-180), With reference to a Saturated Calomel electrode (SCE), the working electrode's potential was assessed. A voltmeter is attached to the working electrode and saturated reference electrode. The first reading was recorded immediately after the samples were immersed in the solution. The voltage was monitored and recorded throughout the entire test period at an interval of 5 minutes .

Electrochemical experiments were also conducted for all samples using a three-electrode cell containing a solution of 3.5% sodium chloride as the electrolyte. The American Society for Testing and Materials GS-87 ASTM [15] states that the counter electrode was the Pt electrode, the reference electrode was SCE, and the working electrode (specimen). They plotted the potentiodynamic polarization curves, which allowed for the estimation of the corrosion potential and corrosion current density (I corr.) using Tafel plots with anodic and cathodic branches. In order to perform the test, the potential was first stepped at a rate of 0.2 mV/s, starting at 250 mV below the open circuit potential and continuing the scan until it reached 250 mV above the open circuit potential. The corrosion rate was measured for each sample according to the following equation:

$$corrosion\ rate\ (mpy) = 0.13\ \frac{I(corr.)(E.W.)}{\rho} \quad \dots\dots\dots\dots (1)$$

3. RESULTS, AND DISCUSSION

3.1. Microstructure

As shown in **Fig. 1(a)**, the microstructure of as-cast AA6111 alloy consists of α-Al dendrites (light phase) with irregular orientations and inter-dendritic regions of the eutectic phase (dark area) formed and distributed between grain boundary and dendrite cell boundary. However, the average grain size was measured at 62μm for casted AA6111 alloy .

After homogenization heat treatment, some inter-metallic compounds distributed between grain and dendrite cell boundary began dissolving in the matrix gradually with increasing temperature and soaking time; as shown in **Fig. 2(a)**, the alloy structure after homogenization treatment possesses grains with an average size of 51 μm. The changes in the microstructure after cold rolling of casted AA6111 alloy, **Fig. 1(b)**, and homogenized AA6111 alloy, **Fig. 2(b)**, were the same. After cold rolling at a reduction rate of 35% of the original thickness, the morphology of the grain transformed progressively from a near-equiaxed shape and homogeneous microstructure to an elongated shape with non-homogeneous microstructure. Also, the cold rolling process reduced the porosity. The effect of the solution heat treatment on the grain structure of these alloys led to recrystallized microstructures. Thus, the AA6111 alloys with and without homogenization possess a refined grain size. Performing the aging treatment after solution treatment and quenching for casted and homogenized AA6111 alloys led to a reduction in the grain size of the alloys with a range of 23-24μm, respectively. Also, it

showed a more homogeneous structure, as shown in **Fig. 1(c)** and **Fig. 2(c).**

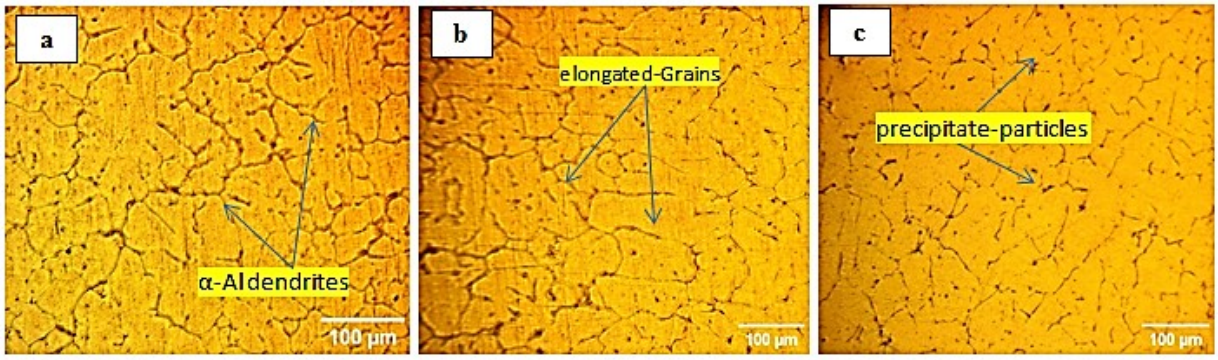

Fig. 1:Microstructure of AA6111 alloy (a) as cast; (b) after rolling; (c) after artificial ageing at 180°C for 10hrs.

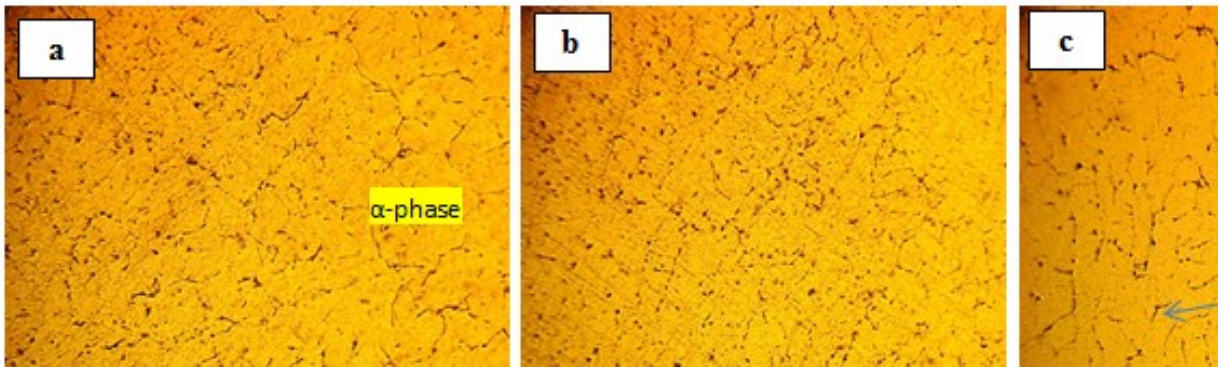

Fig. 2:Microstructure of AA6111 alloy (a) after homogenization; (b) after rolling; (c) after artificial ageing at 180°C for 10hrs.

As shown in **Figs. 1(a)** and **2(a)**, the structure of the casted and homogenized A6111 alloys has a large number of elements that exist in irregular shapes and result in the development of a dendritic network structure.

The alloy's number of components increases with the addition of zirconium, as shown in **Fig. 3(a)**. Thus, the as-cast microstructurewas discernibly refined, with the average grain size of the casted AA6111+0.54wt%Zr alloy determining 35µm.

Because of the presence of intermetallic compounds containing zirconium element, which prevent grain boundaries from moving and from elongating when the rollers apply pressure, the grain shape in **Fig. 3(b)** after the cold rolling process was almost equiaxed and had slight elongation in comparison to the casted or homogenized AA6111 alloy. Following the SHT and aging treatment of the rolled AA6111+0.54wt%Zr alloy, as illustrated in **Fig. 3(c)**, the deformed grains were replaced by a new set of unstressed and fresh grains, with an average grain size of 10µm after artificial aging.

Because of the precipitation of fine intermetallic compounds or particles containing zirconium elements owing to Zener pinning, the recrystallization process in this alloy is considerably slowed down.

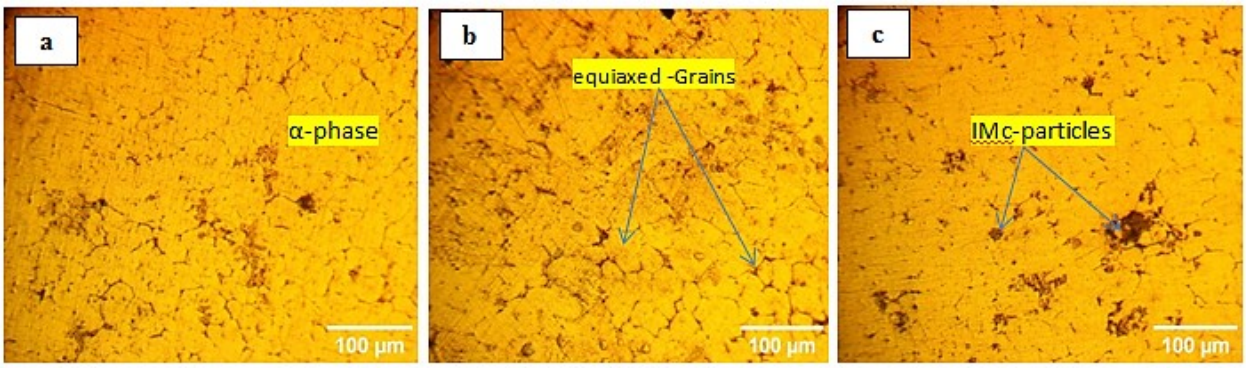

Fig. 3:Microstructure of AA6111+0.54%Wt%Zr alloy (a) as cast; (b) after rolling; (c) after artificial ageing at 180°C for 10hrs.

From **Fig. 4**, which shows the average particle size measured for all alloys at different conditions, it is noted that the average grain size of the casted AA6111 alloy was (62µm). In comparison, the average grain size of this alloy decreased with the addition of zirconium to 35µm.

Homogenization treatment has little effect on the average grain size of the as-cast AA6111 alloy, which was (51µm). The average grain size after cold rolling decreases significantly for all alloys, and with increasing rolling deformation, the concentration of dislocations and their intersection with other dislocations or with secondary phase particles increases. Thus, a high density of dislocation nets can result in the formation of the tiny subgrain through the rotation and breaking of the original grain.The decrease in the average grain size after artificial aging may be because, during solution treatment, new grains that were smaller than the original grains were formed as a result of the dissolution of the intermetallic compounds that were present in the structure. These grains do not have enough time to grow and, therefore, remain smaller in size compared to the size of the original grains after artificial aging.

In general, the results indicated that the best grain refinement was due to the addition of the Zr alloying element. **Fig. 5** illustrates a sample of plots obtained by using Image-J and Origin-Pro 2024b analysis programs.

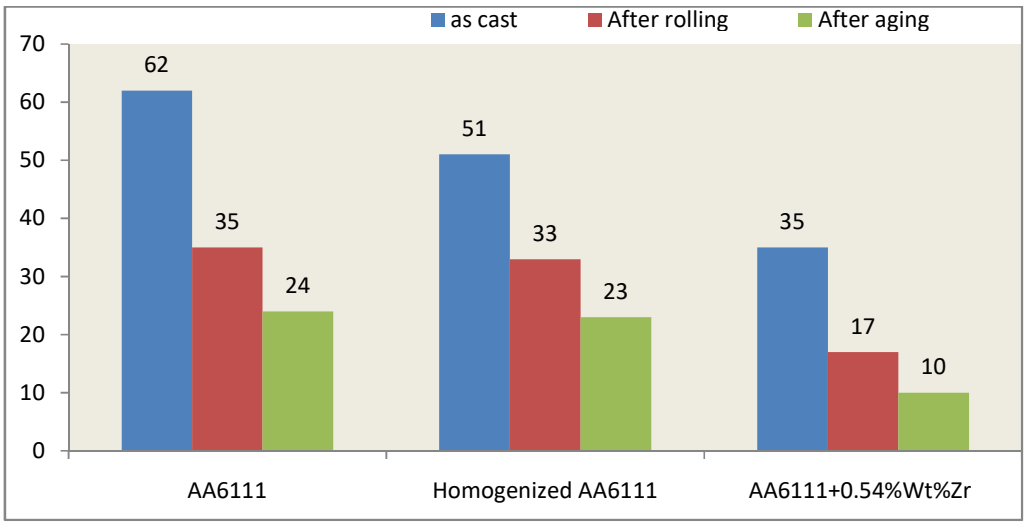

Fig. 4: The average grain size for all alloys at different conditions.

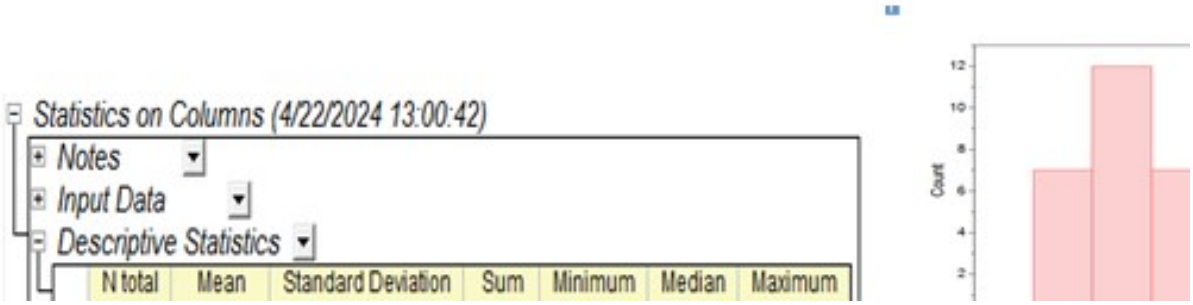

Fig. 5: Average grain size for AA6111+0.54%Wt%Zr alloyafter cold rolling by Image-J and Origin-Pro 2024b analysis programs.

3.2. X-Ray Diffraction (XRD)

Fig. 6 displays the X-ray diffraction (XRD) patterns of the AA6111 alloy after artificial aging. The peaks seen in the patterns correspond to the Mg2Si phase, as indicated by the standard reference codes (35-0773, 34-0673). The X-ray diffraction (XRD) patterns of the AA6111+0.54%Wt%Zr alloy, as seen in **Fig. 7**, exhibit peaks that are consistent with the conventional reference codes (02-1093, 34-0673) for the Al3Zr and Mg2Si phases.

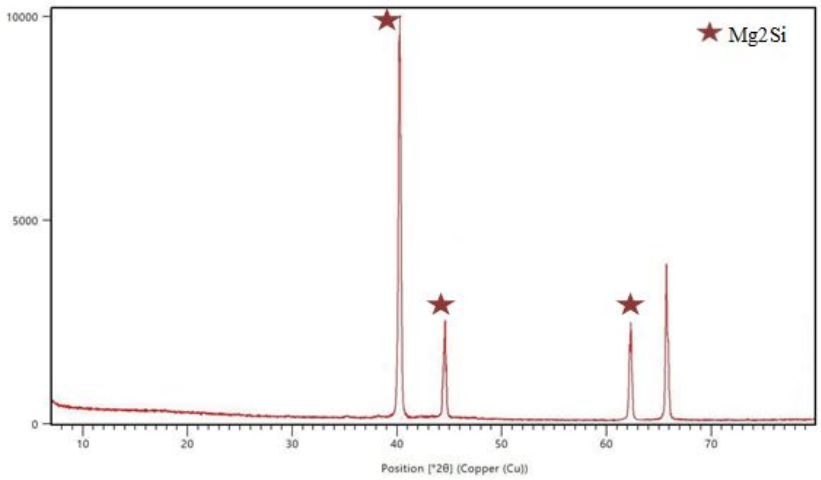

Fig. 6: XRD analysis of the AA6111 alloy after artificial ageing at 180°C for 10hrs.

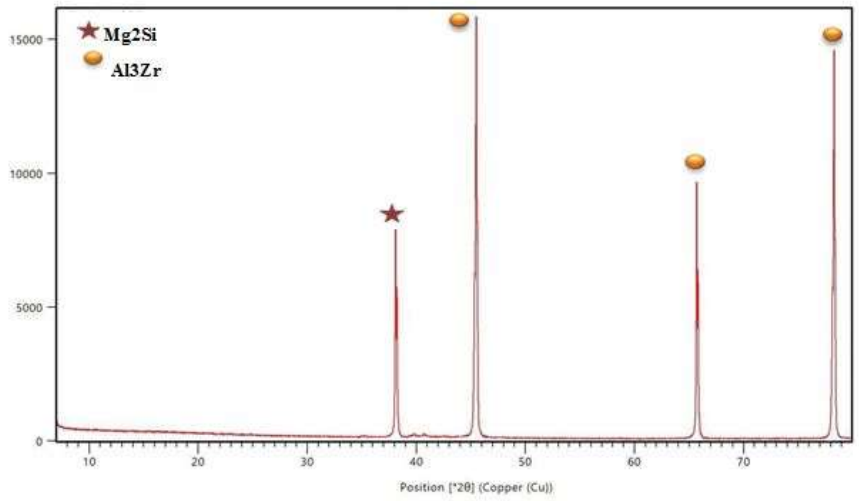

Fig. 7: XRD analysis of the AA6111+0.54%Wt%Zr alloy after artificial ageing at 180°C for 10hrs.

The AA6111 and AA6111+0.54WT%Zr alloys undergo phase transformation throughout the casting process. After solution treatment at an appropriate temperature and time, followed by cooling in ice, the alloys are artificially aged under controlled heating conditions for an extended period of time. The occurrence of phase changes in these phases substantially influences the chemical characteristics of alloys as a whole. Consequently, the existence of these phases has a considerable effect on the corrosion resistance.

3.3. Energy Dispersive X-Ray Analyzer (EDX)

In this study, AA6111, AA6111+0.54wt%Zr alloys were analyzed, this test was done by using etching solution. **Fig. 8** shows the EDS analysis of aged AA6111 alloy. The results confirm the presence of Mg and Si elements as the main components of the Mg_2Si phase. Small amounts of Cu and Fe were also visible. EDS analysis of the aged AA6111+0.54wt%Zr alloy indicates that the Zr was successfully precipitated, as shown in **Fig. 9**, is the main component of the Al_3Zr phase, with apparent weight ratios of silicon and copper.

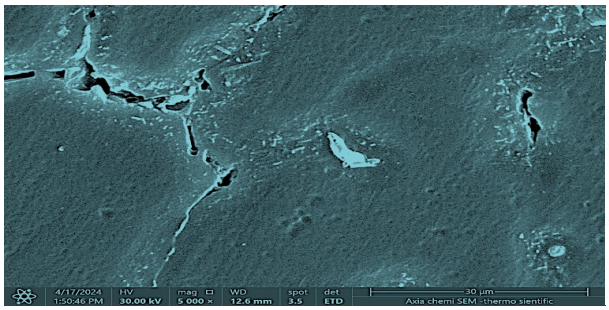

Element	Atomic %	Weight %
Mg	0.1	0.2
Al	55.7	70.7
Si	1.4	1.9
Fe	0.3	0.8
Cu	0.6	1.9

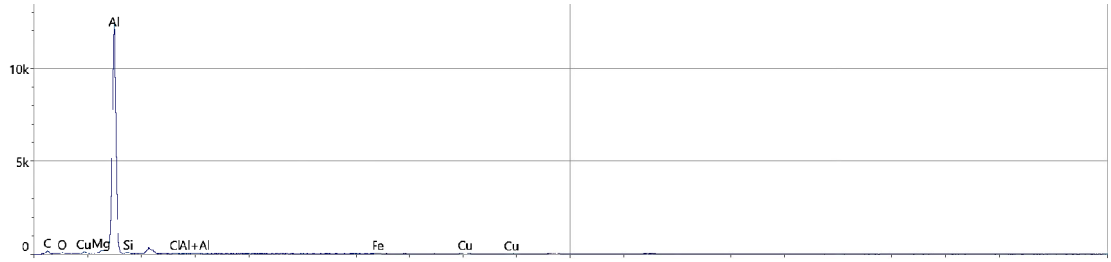

Fig. 8: EDS analysis for aged AA6111 alloy.

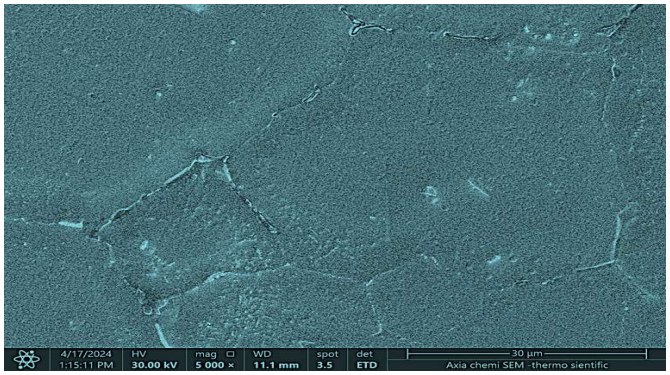

Element	Atomic %	Weight %
Al	96.1	94.5
Si	3.0	3.0
Cu	0.6	1.3
Zr	0.3	1.1

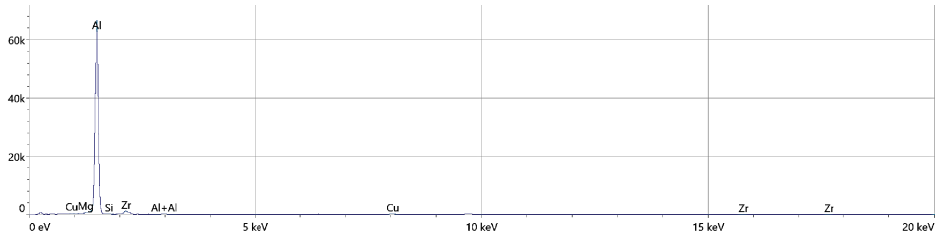

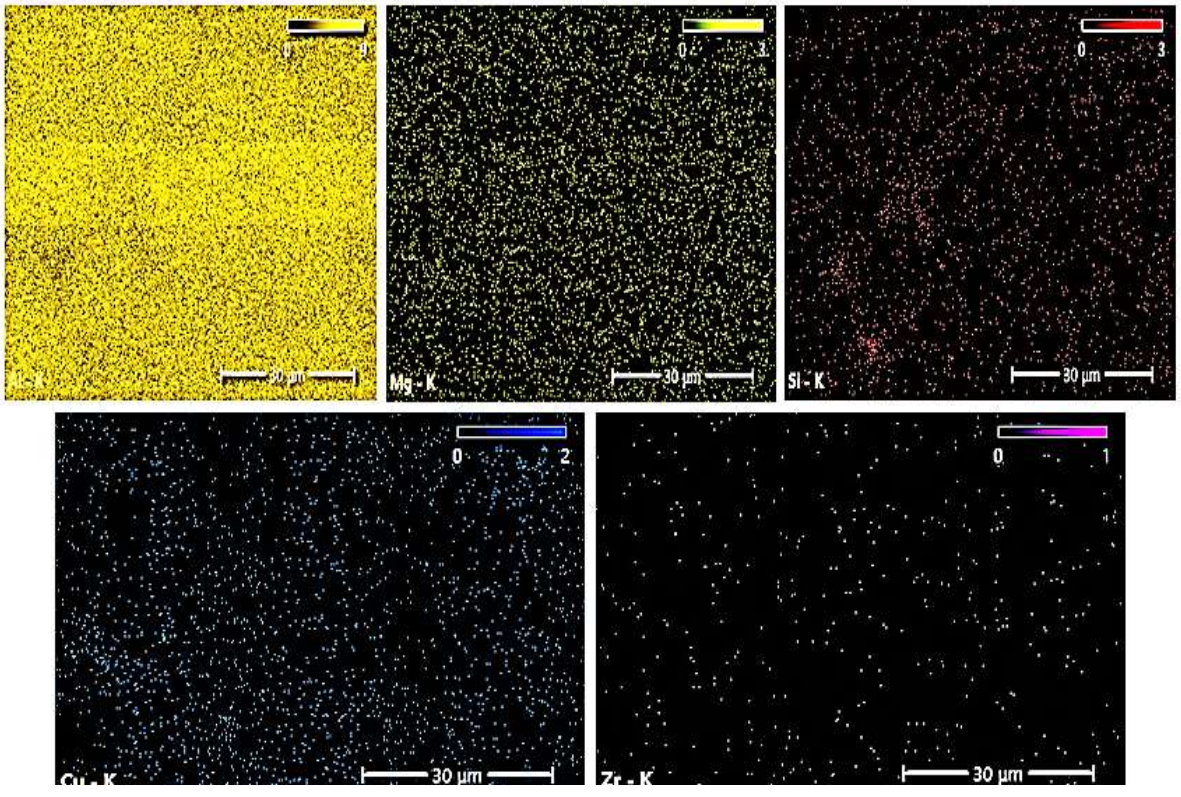

Knowing the behavior of AA6111 alloys in a neutral chloride environment which might be more representative of automotive exposure conditions than the acidic chloride environment, is essential. The stability of the AA6111+0.54wt%Zr was compared to that of the AA6111 alloy by measuring the open-circuit potential versus time concerning SCE until a constant value was reached. **Fig. 10** shows the variations of potential from immersion in the NaCl solution with a time and the tendency to a steady-state value. The open circuit potential is enhanced in the AA6111+0.54wt%Zr alloy, which has a lower value than AA6111alloy. The **Fig** shows a shift towards the less negative potential, which seems related to the formation and thickness of the oxide layer on the metal surface, which improves its corrosion resistance. The EOCP slowly increases, indicating that the film is growing on the metal surface. After being submerged, the samples were in the solutions for more than 50 minutes, and the samples tested exhibited no signs of potential drops associated with surface activation.

The OCP of the AA6111 alloy in 3.5% Sodium Chloride solution was(-296mV) for the alloy without homogenization (A1) and (-325mV) for the AA6111 alloy with homogenization (A2), and the potential value decreases with the addition of zirconium to the AA6111 alloy. AA6111+0.54wt%Zr alloy showed the least negative potential readings(-109mV), as shown in **Table 2**.

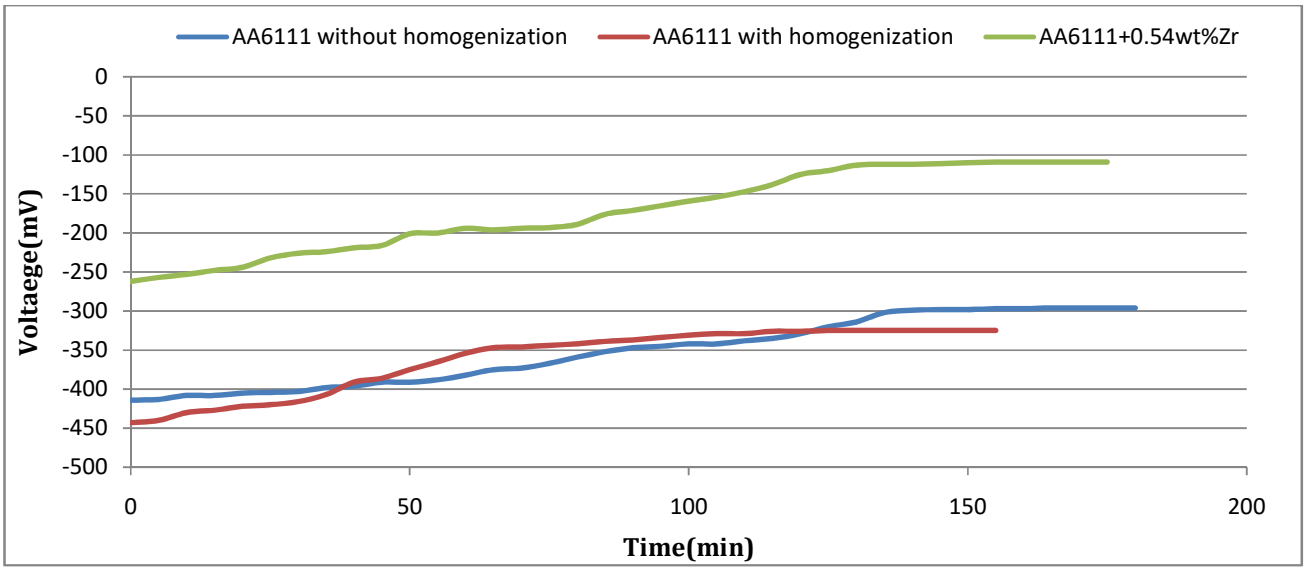

Fig. 10: OCP-time for all alloys after artificial ageing at 180°C for 10hrs in 3.5% sodium chloride solution.

Table 2: EOCP and improvement percentage for all alloys

Sample	$E_{OCP.}$(mV)	Improvement percentage %
AA6111 without homogenization (A1)	-296	---------
AA6111 with homogenization (A2)	-325	---------
AA6111+0.54wt%Zr	-109	66.46

4.2. Potentiodynamic polarization

Utilizing potentiodynamic polarization to estimate corrosion behavior of all alloys used in 3.5% sodium chloride solution. Corrosion test results for the specimens in the mentioned solution at room temperature are shown in **Table. 3**, as the corrosion parameters which are corrosion current (Icorr.), corrosion potential (Ecorr.), and (corrosion rate).

Table. 3 shows that there was a significant improvement in corrosion resistance of the AA6111+0.54Wt%Zr and Icorr. for AA6111+0.54wt%Zr alloy without homogenization was graded in a decrease to 0.76μA for AA6111+0.54wt%Zr alloy without homogenization which was lower than (Icorr.) for AA6111 alloy with and without homogenization which were 2.25μA and 2.86μA respectively. However, the (Ecorr.) value for AA6111+0.54wt%Zr alloy was increased to +28mV for AA6111+0.54wt%Zr alloy than (Ecorr.) for AA6111 without homogenization and with homogenization which was -26mV and -82mV respectively.

Table 3, shows improvement in corrosion resistance of AA6111 alloys with the addition of zirconium. However, adding zirconium to the AA6111 alloy led to a significant decrease in the corrosion rate and current, as shown in **Fig. 11**.

The degree of heat treatment has an impact on the corrosion mechanism. Therefore, the corrosion resistance of AA6111 pre-homogenized alloy is lower compared to non-homogenized alloy.

The low corrosion resistance of AA6111 alloy may be attributed to the presence of cathodic sites in the aluminum matrix: iron-rich intermetallics [**16**-**18**]; silicon-enriched remnants of Mg2Si [**16**, **18**, **19**]; and redistributed copper on the alloy surface [**20**], which lead to the dissolution of the surrounding matrix during polarization.

Table. 3: Electrochemical parameters for all used alloys in 3.5% sodium chloride solution.

Samples	I corr. (μA)	Ecorr. (mV)	Corrosion rate (mpy)	Improvement percentage %
AA6111 without homogenization	2.25	-26	12.918×10^{-3}	---------
AA6111 with homogenization	2.86	-82	16.074×10^{-3}	---------
AA6111+0.54wt%Zr	0.763	28	4.416×10^{-3}	72.53

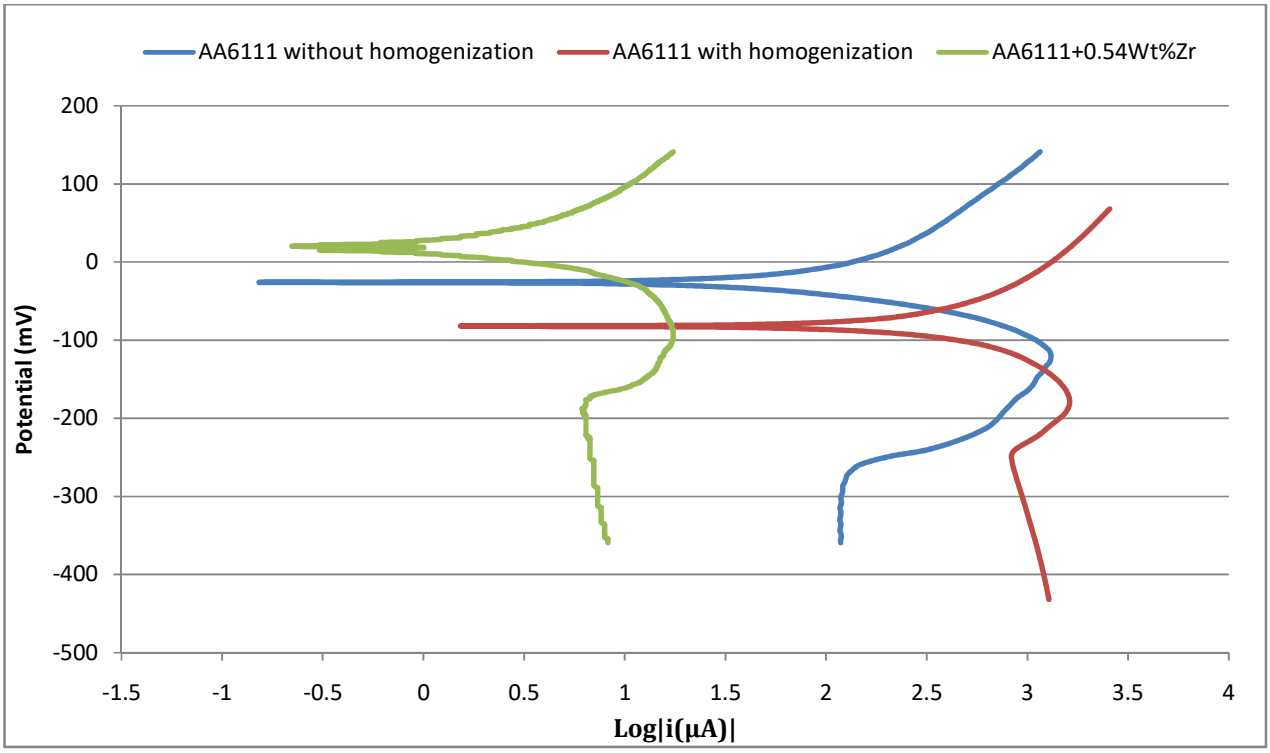

Fig. 11: Potentiodynamic polarization for all alloys after artificial ageing at 180°C for 10hrs in 3.5% sodium chloride solution.

Corrosion in the AA6111 alloy may occur due to two distinct causes. One factor that may prevent the corrosion of AA6111 in neutral atmospheres is the presence of protective passive oxide films. Localized damage to passive films will result in accelerated corrosion. The second reason stems from the presence of alloying elements within this alloy. Any different metals found in this alloy, whether impurities or alloying elements, will combine with aluminum to produce inter-metallic compounds. When the electrochemical potentials of these intermetallic (IM) compounds differ from the Al matrix, there will be variations in the local currents on the alloy's surface. The micro-galvanic reaction produces anodes and cathodes.

IM particles in the AA6111 alloy induce two distinct forms of localized corrosion behavior, as shown by **[21]**. The first phenomenon involves the formation of circumferential pits, which manifest as a ring of corrosion around IM particles that are more chemically resistant than the surrounding Al matrix.

The second shape involves the preferential dissolution of particulate matter that is more reactive as intermetallic (IM) particles compared to the aluminum (Al) matrix.

The addition of zirconium into the AA6111 alloy has enhanced its corrosion resistance. The primary purpose of adding zirconium to this alloy was to enhance the refining of the grain size. A recent work (Kim et al., 2018) proposed that the corrosion property is impacted by both the size and amount of intermetallic compounds present in the Al matrix. Therefore, the correlation between the corrosion characteristics of the AA6111 alloy and the increase in both particle number and size should be considered. The corroded regions around the Mg2Si particles observed in the AA6111 alloy may exhibit an overlapping structure, resembling a 'net structure. Therefore, the uninterrupted distribution of these IMc is accountable for the

continuous formation of corrosion in this alloy. In the AA6111+0.54wt%Zr alloy, the existence of Al3Zr particles might impede the growth of grains and enhance the nucleation of other precipitate particles (Mg2Si) during solution heat treatment. Consequently, the particle size of inter-metallic compounds around Al3Zr grows finer, and the dispersal increases. Therefore, the addition of Zr may refine and disperse corrosive IM particles, thus decreasing the localized propagation of corrosion in the AA6111 alloy.

5. CONCLUSION

This study investigated how adding zirconium affected the corrosion properties of the rolled and artificially aged AA6111 alloy. The immersion corrosion test revealed that alloys containing zirconium exhibit significantly less corrosion spread. The open circuit potential (OCP) time measurement test indicates a decrease in the open circuit potential value with zirconium addition, with the AA6111+0.54wt%Zr alloy demonstrating the least negative potential readings (-109 mV) when compared to the AA6111 alloy, both with and without homogenization. The corrosion behavior of all alloys was also studied by performing potentiodynamic polarization in a 3.5 sodium chloride solution, where it was noted that the corrosion rate as well as the value of the corrosion current decreased when zirconium was added to the AA6111 alloy. The percentage improvement in corrosion resistance in the AA6111+0.54wt%Zr alloy reached 72.53%.

6. ACKNOWLEDGEMENT

The authors express their gratitude for the financial assistance provided to the Metallurgical Engineering Department of Materials Engineering College. I would like to extend my profound gratitude to the laboratory personnel at Babylon University for their invaluable support.

7. REFERENCES

1. Davis, J. R. (Ed.). (2001). Alloying: Understanding the basics . ASM International.

2. Frankel, G. S. (1998). Pitting corrosion of metals: A review of the critical factors. Journal of the Electrochemical Society, 145 (6), 2186.

3. Davis, J. R. (Ed.). (1999). Corrosion of aluminum and aluminum alloys . ASM International.

4. Shercliff, H. R., & Ashby, M. F. (1990). A process model for age hardening of aluminum alloys—I. The model. Acta Metallurgica et Materialia, 38 (10), 1789-1802.

5. Birbilis, N., & Buchheit, R. G. (2005). Electrochemical characteristics of intermetallic phases in aluminum alloys: An experimental survey and discussion. Journal of the Electrochemical Society, 152 (4), B140.

6. Mukhopadhyay, P. (2012). Alloy designation, processing, and use of AA6XXX series aluminum alloys. International Scholarly Research Notices, 2012 (1), 165082.

7. Cole, G. S., & Sherman, A. M. (1995). Light weight materials for automotive applications. Materials Characterization, 35 (1), 3-9.

8. Adapala, P., Hosking, N., Nichols, M., & Frankel, G. S. (2022). Laboratory accelerated cyclic corrosion testing and on-road corrosion testing of AA6××× coupled to carbon fiber-reinforced plastics. Corrosion, 78 (7), 599-611.

9. Larsen, M. H., Walmsley, J. C., Lunder, O., & Nisancioglu, K. (2009). Effect of excess silicon and small copper content on intergranular corrosion of 6000-series aluminum alloys. Journal of the Electrochemical Society, 157 (2), C61.

10. Larsen, M. H., Walmsley, J. C., Lunder, O., Mathiesen, R. H., & Nisancioglu, K. (2008). Intergranular corrosion of copper-containing AA6x xx AlMgSi aluminum alloys. Journal of the Electrochemical Society, 155 (11), C550.

11. Duan, C., Tang, J., Ma, W., Ye, L., Jiang, H., Deng, Y., & Zhang, X. (2020). Intergranular corrosion behavior of extruded 6005A alloy profile with different microstructures. Journal of Materials Science, 55 , 10833-10848.

12. Xuehong, X., Deng, Y., Shuiqing, C., & Xiaobin, G. (2020). Effect of interrupted ageing treatment on the mechanical properties and intergranular corrosion behavior of Al-Mg-Si alloys. Journal of Materials Research and Technology, 9 (1), 230-241.

13. Zedin, N. (2022). Effect of quenching treatment on corrosion behavior and mechanical properties of 6061 aluminum alloy: Effect of quenching treatment on corrosion behavior and mechanical properties of 6061 aluminum alloy. Wasit Journal of Engineering Sciences, 10 (2), 185-192.

14. Onat, A. (2018). Effects of artificial aging heat treatment on mechanical properties and corrosion behaviour of AA6XXX aluminium alloys. Journal of Chemical Engineering and Materials Science, 9 (2), 17-23.

15. ASTM. (2004). Standard practice for calculation of corrosion rates and related information from electrochemical measurements (G102-89). ASTM International, West Conshohocken, USA.

16. Andreatta, F., Turco, A., De Graeve, I., Terryn, H., de Wit, J. H. W., & Fedrizzi, L. (2007). SKPFM and SEM study of the deposition mechanism of Zr/Ti-based pre-treatment on AA6016 aluminum alloy. Surface and Coatings Technology, 201 , X.

17. Jain, S., Hudson, J. L., & Scully, J. R. (2013). Effects of constituent particles and sensitization on surface spreading of intergranular corrosion on a sensitized AA5083 alloy. Electrochimica Acta, 108 , 253-264.

18. Paussa, L., Andreatta, F., Navarro, N. R., Durán, A., & Fedrizzi, L. (2012). Study of the effect of cerium nitrate on AA2024-T3 by means of electrochemical micro-cell technique. Electrochimica Acta, 70 , 25-33.

19. Eckermann, F., Suter, T., Uggowitzer, P. J., Afseth, A., & Schmutz, P. (2008). The influence of MgSi particle reactivity and dissolution processes on corrosion in Al–Mg–Si alloys. Electrochimica Acta, 54 (2), 844-855.

20. Mol, J. M. C., Hinton, B. R. W., Van Der Weijde, D. H., De Wit, J. H. W., & Van Der Zwaag, S. (2000). A filiform corrosion and potentiodynamic polarisation study of some aluminium alloys. Journal of Materials Science, 35 , 1629-1639.

21. Godlewska, E. (2006). Effect of molybdenum on high-temperature corrosion of Fe-Al intermetallics. Intermetallics, 14 , 280-286.